$Na_2SO_4 \cdot 10H_2O$ dehydration in view of thermal storage

Chemical Engineering Science 134 (2015) 360–366

Contents lists available at ScienceDirect

Chemical Engineering Science

journal homepage: www.elsevier.com/locate/ces

$Na_2SO_4 \cdot 10H_2O$ dehydration in view of thermal storage

P.A.J. Donkers [a,c], K. Linnow [d], L. Pel [a,*], M. Steiger [d], O.C.G. Adan [a,b]

[a] Technical University Eindhoven, Den Dolech 2, 5600 MB Eindhoven, The Netherlands
[b] TNO Building and Construction Research, PO Box 49, 2600 AA Delft, The Netherlands
[c] M2i, Mekelweg 2, 2600 GA Delft, The Netherlands
[d] University of Hamburg, Martin-Luther-King-Platz 6, 20146 Hamburg, Deutschland

HIGHLIGHTS

- We studied the dehydration of mirabilite with help of NMR, XRD and Raman.
- The phase transformation from mirabilite into thenardite is observed to be a one-to-one process.
- No metastable crystal phases are observed by XRD and Raman during the dehydration process.
- A homogeneous drying process inside the grain is observed.

GRAPHICAL ABSTRACT

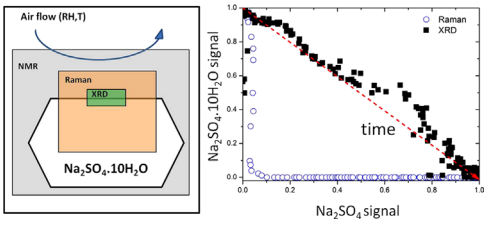

ARTICLE INFO

Article history:
Received 30 March 2015
Received in revised form
13 May 2015
Accepted 18 May 2015
Available online 27 May 2015

Keywords:
Mirabilite
NMR
Raman spectroscopy
X-ray diffraction

ABSTRACT

The idea of using hydrated salts as working media for thermal energy storage has increased the interest in understanding their phase transitions. During studying the phase transition of mirabilite into thenardite, the crystal structure and water content are monitored by three experimental techniques. With the help of NMR, homogeneous drying of mirabilite crystals over the entire grain is observed. According to the drying behavior, the mobility of water molecules should be high inside the grain during dehydration. XRD experiments show that during this phase transition no disordered phase or other metastable phases like $Na_2SO_4 \cdot 7H_2O$ or phase III appear. With Raman spectroscopy, these experiments are repeated at several relative humidities and again no metastable phases are observed.

1. Introduction

Renewable energy is of increasing importance in our modern society, because of the lower environmental impact than conventional energy technology. The drawback of renewable energy systems is the fluctuations of energy production and the mismatch in time between the demand and supply of the energy. Systems that buffer the energy in order to synchronize supply and demand are needed. For thermal energy, no compact systems for longer, seasonal storage that fit into existing building configuration exist. This hampers the full introduction of renewable energy systems. Long-term compact heat storage would enable a major break-through for an effective year round use of solar thermal energy. Principally, heat storage in the lower temperature region can be achieved in the form of sensible heat (e.g. using the thermal heat capacity of water or gravel (N'Tsoukpoe et al., 2009)), or in latent form through phase transitions (Brandstetter, 1988; Telkes, 1980) or thermochemical reactions, like sorptive storage (Alefeld, 1980) or hydration of salts (Goldstein, 1961). The last method has the highest potential as it is (nearly) loss-free and has the highest energy density of these options. It is based on enthalpy change in solid-solid transitions involving reaction of salts with a solvent, such as ammonia (Biltz and Grimm, 1925), water (Garg and Nasim, 1981) or methanol (Offenhartz et al., 1980). The general hydration/dehydration reaction is given by

$$M_{\nu_M}X_{\nu_X}(cr)+\nu_0H_2O(g)\rightleftharpoons M_{\nu_M}X_{\nu_X}\cdot\nu_0H_2O(cr), \quad (1)$$

* Corresponding author.
E-mail address: l.pel@tue.nl (L. Pel).

http://dx.doi.org/10.1016/j.ces.2015.05.028
0009-2509/

where $M_{\nu_M}X_{\nu_X}$ is a salt. This reaction is reversible and can be tuned by the vapor pressure of the solvent. One of the advantages of this method is the low loss of heat during storage: as long as the ingredients are stored separately, no energy is lost to the surroundings. Apart from the application as heat storage material the usage of the dehydration reaction for cooling applications is achievable. The dehydration can be achieved at a particular temperature using a well-considered salt water system and can then sustain the temperature (Aristov, 2007; Ervin, 1977) of the environment at a comfortable value.

Previous studies performed on salt complexes in combination with heat storage are based on techniques like X-ray diffraction (XRD) (Huang et al., 2011), thermogravimetric analysis (TGA) (Zondag et al., 2010; Zhu et al., 2009) and differential scanning calorimetry (DSC) (Huang et al., 2011; Bevers et al., 2006). In most of these studies the mechanism of penetration of water in and out the hydrate is not fully understood. Different ideas are proposed, but no theory fits all hydrates (Makatun and Shchegrov, 1972; Lyakhov and Boldyrev, 1972; Galwey, 2000; Koga and Tanaka, 2002). Each hydrate seems to follow its own dehydration process. Galwey (2000) described in his article six different ways of water evolution type (WET). These types are ordered based on three qualifications. Firstly on the way that water is released, i.e. homogeneously or heterogeneously distributed over the crystal. Secondly on the formation or lack of an intermediate phase during the dehydration reaction and thirdly on the final product whether or not amorphous, crystalline phase or (partially) melted crystal appear.

The aim of the present paper is to improve the understanding of the dehydration process of mirabilite, $Na_2SO_4 \cdot 10\,H_2O$. This salt is selected on the basis of its high theoretical energy storage potential (2.37 GJ m^{-3} based on the complete hydration/dehydration and data provided by Marliacy et al., 2000). The second reason is that the dehydration of mirabilite can be easily achieved at comfort temperature and humidity, therefore mirabilite is a promising candidate for cooling applications of residential and office buildings. The experiments described in this paper focus on dehydration experiments with single crystals and extend to dynamics of the water molecules in the crystal structure and to structural changes. Raman spectroscopy, XRD and nuclear magnetic resonance (NMR) are used. Raman spectroscopy and XRD follow the crystal structure in time, while the NMR technique monitors the water distributions in materials, i.e. inside the crystal in situ.

2. The Na_2SO_4–H_2O system

A profound description of the mirabilite structure characteristics as deduced from X-ray diffraction measurements is given by Ruben et al. (1961), Levy and Lisensky (1978) and Brand et al. (2009). They divided the water molecules into two groups of configuration. The first group consists of 8 of the 10 water molecules and is coordinated to the sodium cation by irregular octahedra. The edges of these octahedra are connected with each other, resulting in a string of water molecules through the crystal structure. The second group consists of the remaining 2 water molecules. These molecules have no coordination classification and have more freedom as the bond strengths of hydrogen are weaker than ion–dipole interactions.

In 1949, Telkes showed that mirabilite, $Na_2SO_4 \cdot 10H_2O$, can be used as phase change material for heat storage. The current study uses a different approach, as we focus on the energy storage by a thermochemical reaction (Goldstein, 1961). In that case, the system stores heat during dehydration of the salt hydrate and generates heat by hydration of the anhydrous salt, thenardite. The reaction is (Wagman et al., 1982)

$$Na_2SO_4 \cdot 10H_2O(s) \rightleftharpoons Na_2SO_4(s) + 10H_2O(g), \quad \Delta H = 522\ \text{kJ/mol}. \tag{2}$$

The phase diagram of the system Na_2SO_4–H_2O (Steiger and Asmussen, 2008) is shown in Fig. 1, in consideration of the thermodynamic stable phases, Na_2SO_4(V) and $Na_2SO_4 \cdot 10H_2O$ and the metastable phases Na_2SO_4(III), $Na_2SO_4 \cdot 7H_2O$. The solid lines represent the equilibria of the stable phases, while the dotted lines represent the metastable equilibria. The dashed line represents the working temperature of our experiments. According to the phase diagram, reaction (2) has an equilibrium humidity of 80.7% at 25 °C. This means that dehydration of mirabilite occurs at relative humidities below the 80.7% or that thenardite hydrates above this humidity. The dehydration or hydration rate of a crystal is partially determined by the difference between the applied and the equilibrium relative humidity. The larger the difference, the higher the dehydration/hydration rate is expected to be. In case the RH is increased above 93.5%, the mirabilite will dissolve. Therefor, mirabilite samples are stable as long as they are stored at 25 °C between 80.7% and 93.5% RH. During dehydration not only thenardite can be formed but also two metastable phases can appear: heptahydrate and phase III. Saidov et al. (2012) and Hamilton et al. (2008) showed that heptahydrate can be formed during evaporation of a solution at low temperatures. The phase diagram shows that formation of the heptahydrate may occur during dehydration of mirabilite below 66% RH at 25 °C. The other metastable phase is phase III, an anhydrous phase. This phase can exist in case of dehydration below 76% RH according to the phase diagram. It is known that during the drying of a Na_2SO_4 solution this phase is formed (Rodriguez-Navarro and Doehne, 1999).

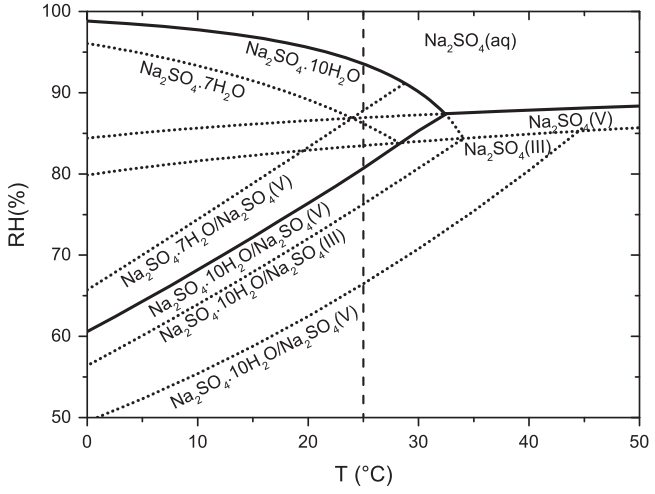

Fig. 1. Phase diagram of Na_2SO_4 in equilibrium with water. The metastable phases are drawn with dotted lines (data from Steiger and Asmussen, 2008).

3. Experimental

3.1. Sample preparation

Crystals of $Na_2SO_4 \cdot 10H_2O$ were grown by slow evaporation of an oversaturated solution at 22 °C. The solution was prepared by cooling down a saturated solution from 40 °C to 22 °C, note that the crystal growth was observed when the solution was already cooled down to 22 °C. The used sizes are based on the limitations of the different experimental setups. For the confocal Raman experiments crystals with a size of about $1 \times 1 \times 0.2\ mm^3$ were used. For the NMR experiments crystals with a size of about $30 \times 5 \times 5\ mm^3$ were selected.

The samples for the XRD experiments were also grown from a solution saturated at 40 °C with Na_2SO_4. The difference is that the solution was poured in the sample holder and placed in a desiccator with a relative humidity of 85% and cooled down to 22 °C. Crystals were grown and residual water was absorbed with a tissue afterwards. This was done to achieve a flat top layer as required for the

XRD measurements. The sample consisted of several crystals lying parallel to each other. The sample holder had an outer diameter of 2.5 cm and a height of 1.5 mm. The sizes of the crystals used were about $10 \times 3 \times 1.5$ mm^3. The crystals were all stored in a box with a relative humidity of 85% at 22 °C.

3.2. NMR

Nuclear magnetic resonance (NMR) is used for measuring non-destructively and quantitatively hydrogen atoms in a sample. NMR is based on the principle that in a magnetic field, nuclei have a specific resonance frequency and can be excited by a radio frequency field. The signal intensity S is given by Vlaardingerbroek and Den Boer (2003)

$$S = k\rho\left(1-\exp\left(-\frac{\tau_r}{T_1}\right)\exp\left(-\frac{\tau_{echo}}{T_2}\right)\right), \quad (3)$$

where k is the sensitivity of the nucleus ($k=1$ for water), ρ the density of the nucleus, τ_r the repetition time of the pulse sequence, τ_{echo} the echo time of the sequence and T_1 and T_2 are the longitudinal relaxation and the transversal relaxation times, respectively. These two relaxation times are properties that depend on the molecular dynamics and structure of the studied nuclei, as well as on the strength and homogeneity of the applied magnetic field (Vlaardingerbroek and Den Boer, 2003).

In this study, two types of NMR measurements were performed; multidimensional correlation (Peemoeller et al., 1981; Galvosas and Callaghan, 2010) and moisture content measurements (Pel et al., 1996). Moisture content profiles were measured on the basis of a Hahn sequence (Hahn and Echoes, 1950). In this sequence, the τ_r is long compared to T_1 and τ_{echo} is short compared to T_2 in order to gain as much signal as possible. Spatial resolution is acquired by applying a static magnetic gradient over the sample.

The T_1-T_2 distribution was measured with a combination of a saturation recovery and a Carl–Purcell–Meiboom–Gill (CPMG) sequence. The saturation recovery sequence measures the longitudinal relaxation (T_1) of a material (Markley, 1971). The sequence saturates the signal and after time τ_1 the signal intensity is measured. The echo at time τ_1 is used as the first echo of the CPMG sequence (Meiboom and Gill, 1958). This sequence measures the transversal relaxation (T_2) of a material. The signal intensity of the first echo at different τ_1 times in combination with the T_2 relaxation measurement was analyzed by a multidimensional inverse Laplace transformation (Song et al., 2002).

The NMR experiments were performed using a home-built NMR setup, which is especially designed for measurements on systems with short relaxation times. A schematic diagram of this setup is shown in Fig. 2. Two coils in anti-Helmholtz configuration are placed 20 cm apart, generating a static gradient of 300 mT/m in the direction of the main magnetic field. A RF-coil in birdcage configuration is used for sending and receiving the NMR signal from the sample. The diameter of the coil is 4 cm and inside the coil a Faraday shield is located. The sample is moved through the RF-coil with a step-motor and a load cell measures the mass real-time during an experiment.

The samples for the T_1-T_2 experiments consisted of stacked crystals in a sealed container with crystals' diameters ranging between 2 and 5 mm. The used crystals are the same crystals as in the dehydration experiment, but crushed to get a higher signal to noise ratio in the NMR. The crystals were placed in a sealed container, wherein a relative humidity of $93 \pm 2\%$ was measured. This value corresponds to the equilibrium RH of mirabilite and its saturated Na_2SO_4 solution at 25 °C. This is probably a result of some remaining droplets of saturated solutions in the crystals aggregate.

During the dehydration experiments, another set of crystals was used with sizes of $30 \times 5 \times 5$ mm^3. Four of them were placed parallel to each other in the sample holder to get more signal during the measurement. The single crystals were sealed with teflon on all sides except the top. In this way the crystal has only one interface in direct contact with its surroundings and water can only escape at that interface. Dry air was blown over the sample at a speed of 1.6 l/min, while the temperature was kept constant at 25 °C.

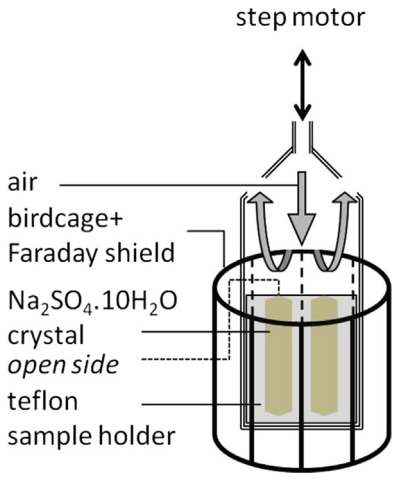

Fig. 2. The NMR setup during the dehydration experiments.

3.3. Raman microscopy

Depolarized Raman spectra were measured with a Senterra Raman spectrometer (Bruker Optics GmbH, Germany) after sample excitation with a 532.0 nm laser and with 20 mW power. The objective used amplifies 20 times, has a NA of 0.4 and a working distance of 10.6 mm. An aperture with a pinhole of 25 μm was used. Spectra between 50 and 1550 cm^{-1} were recorded with an integration time of 5 s and averaged over 4 measurements. The sulfate peak around 990 cm^{-1} is used for analyzing the spectra (Hamilton and Menzies, 2010). The working distance of 10.6 mm was used, because the sample was placed in an environmental chamber, where temperature and relative humidity (RH) were controlled. The temperature was kept constant with a thermostat (DLK and E200, Lauda, Germany) and the relative humidity was generated by an airflow of 500 ml/min produced with a modular humidity generator MGH 32 (ProUmid, Germany). The temperature and RH in the chamber were measured with a RH sensor (Hygroclip SC-05, Rotronic, Germany).

With a Raman experiment, a crystal was placed on a $CaCO_3$ substrate. The laser was focussed 100 μm below the salt–air interface. The initial excitation depth was between 97 and 260 μm below the air–crystal interface according to literature (Juang et al., 1988; Everall, 2000), implying that in the beginning a small signal of $CaCO_3$ can be observed as the crystal thickness is 200 μm. The $CaCO_3$ spectrum was used to assess the effect of the dehydration of the crystal on the Raman signal intensity. The measured spectra were analyzed with the help of the reference spectra of the different phases of sodium sulfate measured by Linnow et al. (2014). The Raman shift of the most intensive $\upsilon 1(SO_4^{2-})$ mode around 980 cm^{-1} was the characteristic for the phase of sodium sulfate as can be seen in Fig. 3. The spectra were analyzed and the contributions of the different phases were calculated. Before starting the dehydration experiment, all grains were equilibrated at 85% RH and 25 °C (i.e. mirabilite is stable) in the environmental chamber. When the spectra were stable during at least 10 min, the RH was changed to the desired value.

3.4. XRD

XRD parameters were obtained on a Siemens D5000 Bragg–Brentano parafocusing powder diffractometer with a vertical θ : 2θ configuration using Cu Kα-radiation and a position-sensitive

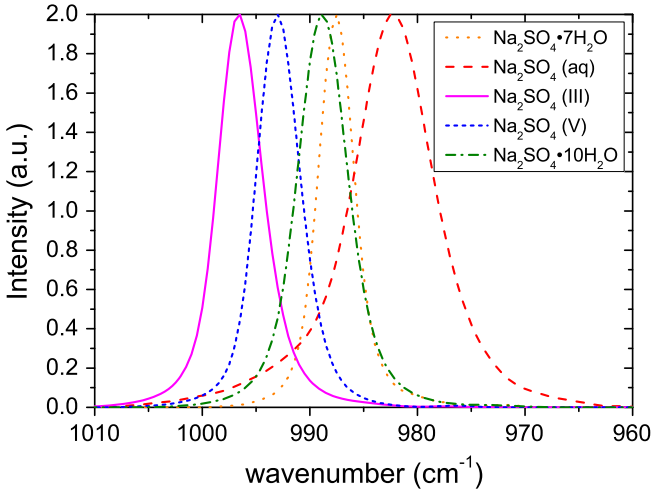

Fig. 3. The reference spectra of the different phases of sodium sulfate (Linnow et al., 2013; Hamilton and Menzies, 2010).

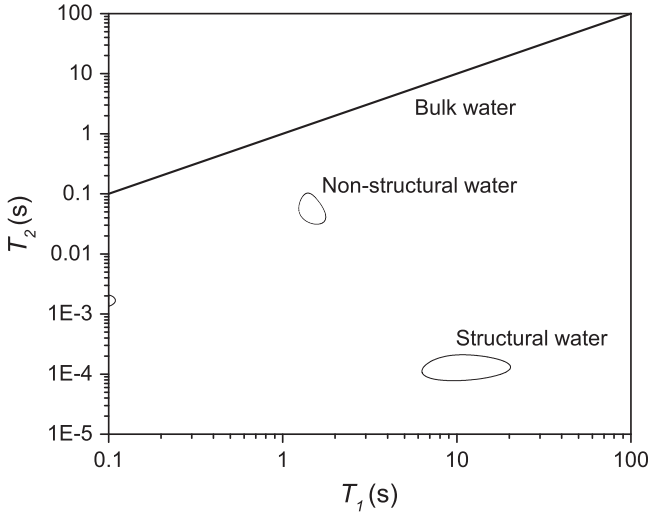

Fig. 4. The T_1-T_2 distribution of the water molecules in Na_2SO_4 is shown. The solid line represents $T_1=T_2$, which corresponds to liquid water molecules in bulk volume.

detector (PSD). The temperature and the RH were controlled by a home-built relative humidity chamber (Linnow et al., 2006).

XRD patterns of the sample were measured from 10 to 70° 2θ and compared with X-ray databases; i.e. pdf 11–647 and 24–1132 (ICCD, 2001). The sample conditioning in the XRD setup was similar to the Raman experiment. The crystals were equilibrated at 25 °C and 85% RH. After the equilibration period, the RH was decreased to 78% and every 15 min a new XRD pattern is recorded.

4. Results and discussion

4.1. NMR

4.1.1. Equilibrium experiments

Fig. 4 shows a T_1-T_2-distribution of the water molecules in $Na_2SO_4\cdot 10\,H_2O$ at 25 °C and 93 ± 2% RH. In the contour plot two peaks can be distinguished, which are labeled as structural water and non-structural water. The black line corresponds to the $T_1=T_2$ line, which is characteristic for water molecules in moderately large reservoirs with a similar freedom as bulk water. The non-structural water peak is placed close to this line, so apparently indicating a high mobility. This high mobility is too large to be related to the two weakly bound water molecules in Na_2SO_4 (Ruben et al., 1961; Levy and Lisensky, 1978; Brand et al., 2009). In addition the peak intensity contributes to only 4% of the total signal intensity, which should be 20% incase it is related to these weakly bound water molecules. In contrast, the other peak is located far from this line, being characteristic of immobile, solid-like or bound water molecules. The difference between the observed structural and non-structural water peak in the NMR experiments is probably caused by imperfections in the crystal structure or adsorbed surface water.

4.1.2. Dehydration experiments

Fig. 5a shows the moisture content profiles recorded during the dehydration experiment of the four parallel crystals. On the vertical axis the moisture content is plotted against the position on the horizontal axis. The measured moisture content is a combination of structural and non-structural water. The open side of the sample is located on the left side of the graph. Each line corresponds to a moisture content profile, with 8 h between two subsequent profiles. Every 100 min, a single profile is measured, but only every fifth profile is plotted. The moisture concentration profile at a specific moment in time is deduced from the experimental data through interpolation of the local moisture concentration as a function of time using least-squares fits with cubic splines. Relaxation analyses were performed during the dehydration experiment, but no significant change of the ratio of structural and non-structural water was found.

The dehydration measurement shows that drying of the single crystal occurs almost homogeneously over the entire sample. After the first 8 h, also at 30 mm from the top of the sample the water level decreased significantly. This implies a very high mobility of the water molecules in the grain. This can be a combination of vapor diffusion and crystal water diffusion. Note that we do not detect water vapor with NMR. We have no clear indication that other phases than mirabilite or thenardite occur during this experiment, see Fig. 5b. The water content drops continuously from 10 to 0 mol water per mol Na_2SO_4 both averaged over the entire crystal, and at a specific position. If an intermediate phase should exist, we would expect a discontinuity in the drying rate. Another option is that the intermediate phase exists relatively briefly. Raman and XRD experiments will clarify this. Note that the NMR experiment measures the average water content in a certain area and not the exact amount of water at a specific position. NMR cannot distinguish between the coexistence of mirabilite and thenardite domains in a volume or of a continuous loss of water molecules in the observed volume. The first 10 mm in the grain show a minor gradient in its water content profiles, which is a result of a combination of the resolution of the NMR and the grain's shape, which is a cuboid with two pyramids on the ends. After the dehydration experiment the sample was visually checked. The mirabilite crystal is dehydrated pseudomorphically by small thenardite crystals during dehydration. This was also observed by Rodriguez-Navarro and Doehne (1999). Their SEM pictures showed a porous structure after dehydration of mirabilite into thenardite. This porous structure might explain the fast water transport through the grain, resulting in the observed homogeneous drying of mirabilite.

What we can conclude from these homogenous profiles is that no reaction interface is observed in case of dehydration of mirabilite inside the grain. This shows that the evaporation rate at the grain–air interface determines the overall dehydration rate. Dehydration of a mirabilite domain has a similar probability across the grain and is not influenced by other domains or locations in the grain. According to the classification of dehydration reactions of Galwey (2000), this system belongs to group WET 4C, homogeneous intracrystalline chemical change.

4.2. X-Ray diffraction

In Fig. 6a XRD patterns collected during the dehydration experiment are plotted. The pattern of the starting material shows

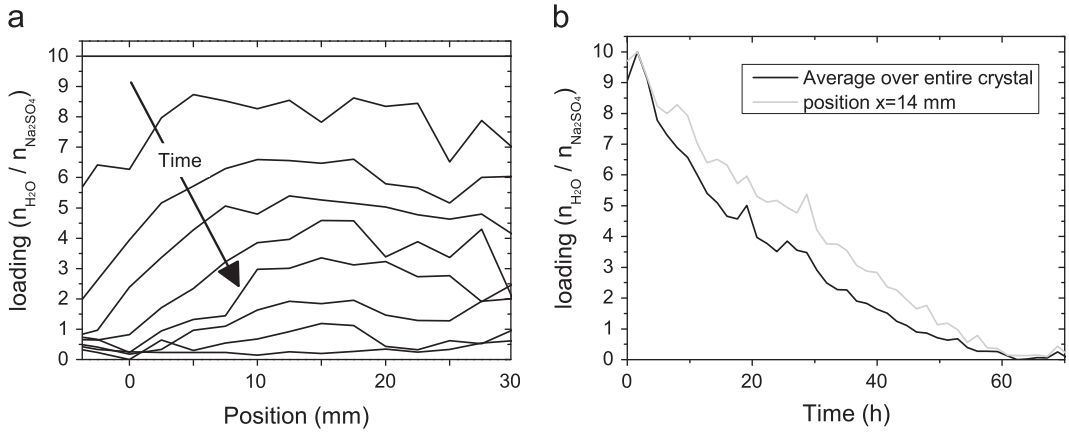

Fig. 5. (a) Water content profiles during the dehydration experiment with four parallel single crystals of Na_2SO_4. On the vertical axis the average concentration of water molecules per mol Na_2SO_4 is plotted versus the position on the horizontal axis. The time between two subsequent profiles is 8 h. After 70 h the sample is completely dry. The arrow indicates the progression in time. (b) The average concentration of water molecules per mol Na_2SO_4 plotted against time at position $x=14$ mm and the average of the entire crystal.

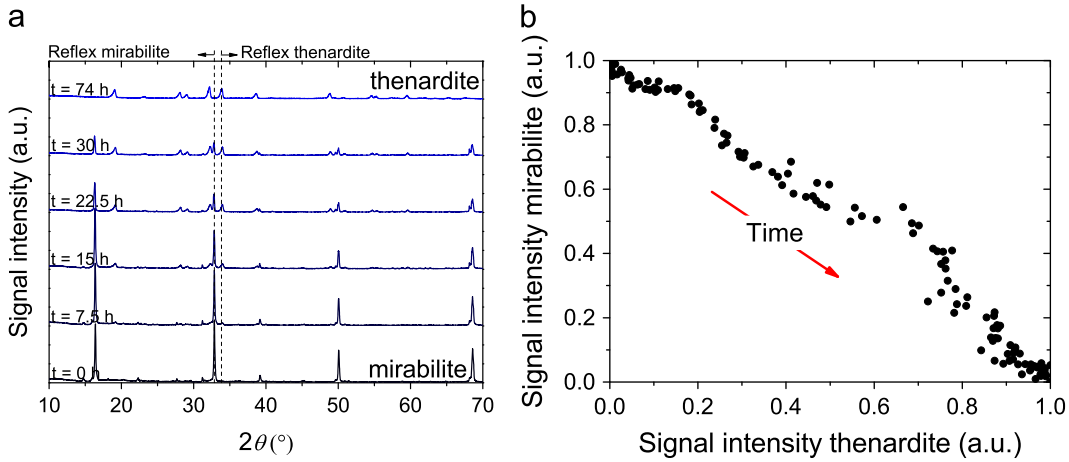

Fig. 6. (a) The XRD patterns during the drying process at different times. The mirabilite signal is converted into thenardite in 74 h. After 36 h already 80% of the mirabilite is converted. The two dashed lines plotted in the graph are the peaks which are used for Fig. 6b. Here, the signal of mirabilite is plotted versus thenardite. It seems that the thenardite and mirabilite signals are one-to-one interchangeable.

only 4 clear peaks instead of the large number reported in the powder diffraction (PDF 11–647 ICCD, 2001). The observed peaks are in accordance with the reference database and the lack of the other peaks is caused by preferential orientation. During the dehydration, mirabilite reflections disappear and others corresponding to thenardite increasingly appear. The final pattern is in good agreement with the reference database of thenardite (PDF 37–1465 ICCD, 2001). We observed that during the dehydration, the sample breaks up into smaller grains, as we observed in our NMR experiment.

In the peaks of Fig. 6a two dashed lines are drawn, which belong to characteristic thenardite and mirabilite peaks. By plotting the signal intensities of these two lines against each other, Fig. 6b is compiled, showing that a one-to-one conversion of mirabilite into thenardite takes place.

4.3. Raman spectra

Fig. 7 shows how the Raman spectra change during dehydration at 25 °C and RH 70%. The signal contributions of the two observed phases, mirabilite and thenardite, are plotted in the inset. Other phases of sodium sulfate, phase III and heptahydrate do not give any signal intensities above the detection limit during this experiment. The mirabilite signal drops to approximately 10% of its original intensity within the first 10 min and afterwards signal growth of thenardite is observed. Similar trends were observed at other depths of focus. This indicates that the dehydration occurs homogenously over the entire sample, with our resolution of 160 μm. By measuring the mass at minimal signal intensity a water content of 8 ± 1 water molecules per $NaSO_4$ molecule was found in the crystal. So a large amount of crystal water is still present in the crystal at the time when no mirabilite signal is observed. At the time of weighing the sample, the crystal surface was whitish. The intensity of the $CaCO_3$ signal slowly disappeared and halfway through the experiment this signal vanished away completely. While $CaCO_3$ is not affected by a RH difference, the observed difference is a result of changes in the crystal on top of the tablet. The laser beam did not reach the $CaCO_3$ anymore, which is probably due to additional air–grain interfaces that increase the path length and the scattering of the beam.

Additional experiments with different RHs showed similar characteristics. In Fig. 8 the time between the start of the experiment and a constant thenardite signal is plotted against the RH. Constant means that the signal did not vary within 10 min. It shows that the time needed for complete dehydration strongly depends on the RH. When the difference between the applied RH and the equilibrium RH of mirabilite and thenardite (80% at 25 °C) decreases, the time needed to reach a constant thenardite signal increases. During all our experiments we did not find any indication of the formation of

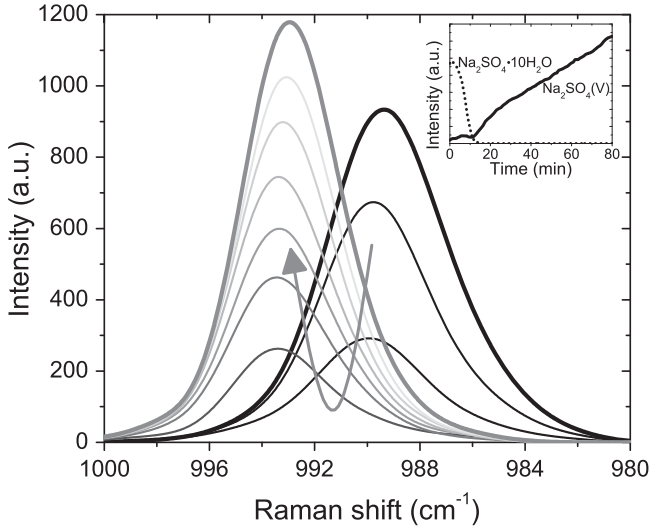

Fig. 7. Part of the Raman spectrum of the grain plotted during a dehydration experiment at RH = 70% at 25 °C. The time between two subsequent lines is 9 min. The inset shows the signal contributions of the components in the grain. The signals are calculated with respect to the signal intensities of the reference spectra.

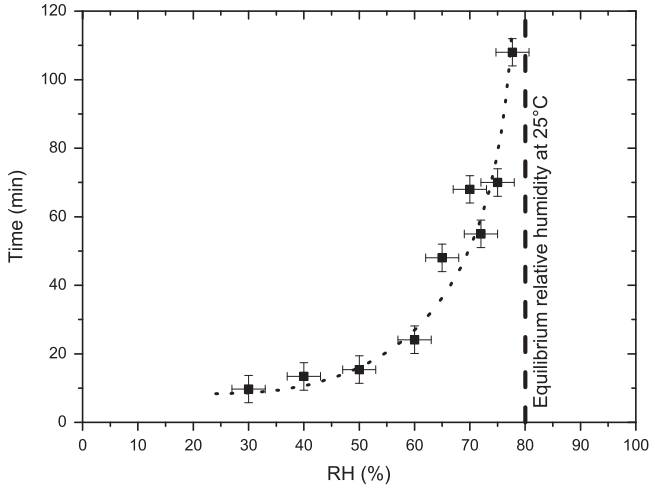

Fig. 8. The time between the start of the dehydration experiment and the maximum thenardite intensity during dehydration experiments at 25 °C is plotted against the applied relative humidity during dehydration.

heptahydrate or phase III. Even in cases where the applied RH is below the equilibrium RH of respectively mirabilite/heptahydrate and mirabilite/phase III, no signs of a heptahydrate or phase III were observed, which is in agreement with the NMR data. The Raman experiments show that the RH only affects the dehydration rate and not the dehydration process itself.

The exact reason for the observed loss of Raman intensity during dehydration is unclear. As stated before, the signal intensity can be affected by the additional air–crystal interfaces. Another explanation is that the vibrations are not measured, because they are partially under the noise level. Furthermore, it is known that the peak can be broader in case of smaller grains, which decreases the peak intensity. It is not clear, however, whether such effects may indeed cause such an extreme decrease of the intensity of the symmetric stretch of the sulfate ion. Our observation of the lost sulfate vibrations is similar to the observation of Brotton and Kaiser (2013) for two other salt hydrates, i.e. $MgSO_4$ and $ZnSO_4$. We think that a similar situation is present in our system, but a satisfying explanation for the observed effect is not found.

4.4. Dehydration time

Comparing the time required for complete dehydration obtained with the three different experimental techniques is complicated, due to variations in sample size, relative humidity and surface to volume ratio. Comparing the XRD experiment with the Raman experiment at the same RH and temperature (78% at 25 °C) shows that the Raman sample dehydrates in 2.5 h (see Fig. 8), while the XRD sample dehydrates in 74 h. An explanation for this difference can be found in the air–crystal surface to volume ratio (S/V) of the samples. Because we have a homogenous drying of the sample, the evaporation at the air–crystal surface is the limiting step in the dehydration process. The volume behind this surface represents the amount of water that has to escape through the surface. The S/V during the XRD and Raman experiments are roughly 0.7 mm^{-1} and 32 mm^{-1}, respectively. Correcting the dehydration times proportional to this surface–volume ratio, a difference in the order of 10 h may reasonably be expected. Considering that only slight deviations in RH may significantly affect the dehydration rate (see Fig. 8), the order of magnitude in differences in dehydration time between XRD and Raman may be related to differences in experimental conditions. The NMR experiments give additional information, where we dehydrated the sample about $\pm$0% RH and at 25 °C. The other experiments were all performed at 30% RH or above. Repeating these experiments at 0% RH is challenging, because of the time resolution in our experiments. Note that the S/V of the NMR experiment is 0.03 mm^{-1}, which is much smaller compared to the others, implying that the long drying time of the NMR even with the low RH is probably caused by the low S/V ratio and not by a different dehydration process.

5. Conclusion

In this research it is shown that combining NMR to measure water concentrations, with XRD and Raman for phase identification, gives additional information about the dehydration behavior of a crystal.

The phase transformation from mirabilite into thenardite is observed to be a one-to-one process (XRD) and nucleation of thenardite not only occurs exclusively at the surface but also in the volume. Besides that, no other crystal phase is observed by XRD and Raman during the phase transformation.

The proposed process is that the dehydration of mirabilite is limited by the air–grain surface. The water molecules are mobile within the grain during dehydration (NMR). The high mobility of water molecules inside the grain compared to the evaporation at the air–grain interface is maybe caused by the white layer on top of the grain, which acts as a barrier for the water vapor. This results in a homogeneous dehydration process inside the grain and shows that the phase transition rate is independent on the position in the grain.

From an application point of view, we showed that mirabilite dehydrates into thenardite without formation of metastable phases as intermediate products. This is useful information for thermal heat storage or cooling applications, as the formation of intermediate phases complicates cyclic processes. So the theoretical energy density storage of the salt is reachable in applications. Still, a systematic research on the understanding of heat flows during dehydration and particulary rehydration reactions are necessary before reactions can be used for heat energy storage.

Acknowledgements

This research was carried out under the project number M75.7.11421 in the framework of the Research Program of the Materials innovation institute (M2i) (http://www.m2i.nl) supported by TNO.

References

Alefeld, G., 1980. Verbesserte oder neue Moglichkeiten zur Kraft-Warme-Umwandlung durch Anwendung neuer Stoffe. Ber. Bunsenges. Phys. Chem 84, 995–1008.

Aristov, Y.I., 2007. New family of solid sorbents for adsorptive cooling: material scientist approach. J. Eng. Thermophys. 16 (2), 63–72.

Bevers, E.R.T., van Ekeren, P.J., Haije, W.G., Oonk, H.a.J., 2006. Thermodynamic properties of lithium chloride ammonia complexes for application inahigh-lifthigh temperature chemical heat pump. J. Therm. Anal. Calorim. 86 (3), 825–832.

Biltz, W., Grimm, H.G., 1925. Uber die Gitterenergien von Ammoniakaten. Z. Anorg. Allg. Chem. 145 (1), 63–87.

Brand, H.E.A., Fortes, A.D., Wood, I.G., Knight, K.S., Vočadlo, L., 2009. The thermal expansion and crystal structure of mirabilite (Na2SO410D2O) from 4.2 to 300 K, determined by time-of-flight neutron powder diffraction. Phys. Chem. Miner. 36 (1), 29–46.

Brandstetter, A., 1988. On the stability of calcium chloride hexahydrate in thermal storage systems. Sol. Energy 41 (2), 183–191.

Brotton, S.J., Kaiser, R.I., 2013. In Situ Raman spectroscopic study of gypsum ($CaSO_4.2H_2O$) and epsomite ($MgSO_4.7H_2O$) dehydration utilizing an ultrasonic levitator. J. Phys. Chem. Lett. 4 (4), 669–673.

Ervin, G., 1977. Solar heat storage using chemical reactions. J. Solid State Chem. 22 (1), 51–61.

Everall, N.J., 2000. Confocal Raman microscopy: why the depth resolution and spatial accuracy can be much worse than You think. Appl. Spectrosc. 54 (10), 1515–1520.

Galvosas, P., Callaghan, P.T., 2010. Multi-dimensional inverse Laplace spectroscopy in the NMR of porous media. C. R. Phys 11 (2), 172–180.

Galwey, A.K., 2000. Structure and order in thermal dehydrations of crystalline solids. Thermochim. Acta 355 (1–2), 181–238.

Garg, H., Nasim, M., 1981. Studies on low-temperature salt-hydrate for thermal storage applications. Energy Convers. Manag. 21 (2), 125–130.

Goldstein, M., 1961. Some physical–chemical aspects of heat storage. In: UN Conference on New Sources of Energy, Rome. Paper E/CONF, pp. 411–417.

Hahn, E., Echoes, Spin., 1950. Phys. Rev. 80 (4), 580–594.

Hamilton, A., Menzies, R.I., 2010. Raman spectra of mirabilite, $Na_2SO_4.10H_2O$ and the rediscovered metastable heptahydrate, $Na_2SO_4.7H_2O$. J. Raman Spectrosc. 41 (9), 1014–1020.

Hamilton, A., Hall, C., Pel, L., 2008. Sodium sulfate heptahydrate: direct observation of crystallization in a porous material. J. Phys. D: Appl. Phys. 41 (21), 212002.

Huang, Q., Lu, G., Wang, J., Yu, J., 2011. Thermal decomposition mechanisms of $MgCl_2.6H_2O$ and $MgCl_2.H_2O$. J. Anal. Appl. Pyrolysis 91 (1), 159–164.

ICCD, 2001. PDF-2 2001 (Database), International Centre for Diffraction Data. Newtown Square, PA, USA.

Juang, C.-B., Finzi, L., Bustamante, C.J., 1988. Design and application of a computer-controlled confocal scanning differential polarization microscope. Rev. Sci. Instrum. 59 (11), 2399.

Koga, N., Tanaka, H., 2002. A physico-geometric approach to the kinetics of solid-state reactions as exemplified by the thermal dehydration and decomposition of inorganic solids. Thermochim. Acta 388, 41–61.

Levy, H.A., Lisensky, G.C., 1978. Crystal structures of sodium sulfate decahydrate (Glauber's Salt) and sodium tetraborate decahydrate (Borax). Redetermination by neutron diffraction. Acta Crystallogr. Sect. B 34, 3502–3510.

Linnow, K., Zeunert, A., Steiger, M., 2006. Investigation of sodium sulfate phase transitions in a porous material using humidity- and temperature-controlled X-ray diffraction. Anal. Chem. 78 (13), 4683–4689.

Linnow, K., Steiger, M., Lemster, C., Clercq, H., Jovanović, M., 2013. In situ Raman observation of the crystallization in $NaNO_3$-Na_2SO_4-H_2O solution droplets. Environ. Earth Sci. 69 (5), 1609–1620.

Linnow, K., Niermann, M., Bonatz, D., Posern, K., Steiger, M., 2014. Experimental studies of the mechanism and kinetics of hydration reactions. Energy Procedia 48, 394–404.

Lyakhov, N., Boldyrev, V., 1972. Kinetics and mechanism of the dehydration of crystal hydrates. Russ. Chem. Rev. 41 (11), 919–928.

Makatun, V., Shchegrov, L., 1972. State of water in inorganic crystal hydrates and the characteristic features of their dehydration. Russ. Chem. Rev. 41 (11), 905–918.

Markley, J.L., 1971. Spin-lattice relaxation measurements in slowly relaxing complex spectra. J. Chem. Phys. 55 (7), 3604.

Marliacy, P., Solimando, R., Bouroukba, M., Schuffenecker, L., 2000. Thermodynamics of crystallization of sodium sulfate decahydrate in H_2O – NaCl – Na_2SO_4 : application to $Na_2SO_4.10H_2O$-based latent heat storage materials. Thermochim. Acta 344, 85–94.

Meiboom, S., Gill, D., 1958. Modified spin-echo method for measuring nuclear relaxation times. Rev. Sci. Instrum. 29 (8), 688.

N'Tsoukpoe, K.E., Liu, H., le Pierrès, N., Luo, L., 2009. A review on long-term sorption solar energy storage. Renew. Sust. Energy Rev. 13 (9), 2385–2396.

Offenhartz, P.O., Brown, F.C., Mar, R.W., Carling, R.W., 1980. A heat pump and thermal storage system for solar heating and cooling based on the reaction of calcium chloride and methanol vapor. J. Sol. Energy Eng. 102 (1), 59–65.

Peemoeller, H., Shenoy, R.K., Pintar, M.M., 1981. Two-dimensional NMR time evolution correlation spectroscopy in wet lysozyme. J. Magn. Reson. 45 (2), 193–204.

Pel, L., Kopinga, K., Brocken, H., 1996. Determination of moisture profiles in porous building materials by NMR. Magn. Reson. Imaging 14 (7–8), 931–932.

Rodriguez-Navarro, C., Doehne, E., 1999. Salt weathering: influence of evaporation rate, supersaturation and crystallization pattern. Earth Surf. Process. Landf. 24 (3), 191–209.

Ruben, H.W., Templeton, D.H., Rosenstein, R.D., Olovsson, I., 1961. Crystal structure and entropy of sodium sulfate decahydrate. J. Am. Chem. Soc. 83 (4), 820–824.

Saidov, T.A., Espinosa-Marzal, R.M., Pel, L., Scherer, G.W., 2012. Nucleation of sodium sulfate heptahydrate on mineral substrates studied by nuclear magnetic resonance. J. Cryst. Growth 338 (1), 166–169.

Song, Y.-Q., Venkataramanan, L., Hürlimann, M.D., Flaum, M., Frulla, P., Straley, C., 2002. T(1)–T(2) correlation spectra obtained using a fast two-dimensional Laplace inversion. J. Magn. Reson. 154 (2), 261 8.

Steiger, M., Asmussen, S., 2008. Crystallization of sodium sulfate phases in porous materials: the phase diagram Na_2SO_4-H_2O and the generation of stress. Geochim. Cosmochim. Acta 72 (17), 4291–4306.

Telkes, M., 1980. Thermal energy storage in salt hydrates. Sol. Energy Mat. 2 (4), 381–393.

Vlaardingerbroek, M.T., Den Boer, J.A., 2003. Magnetic Resonance Imaging: Theory and Practice, 3rd edition, Springer-Verlag, Berlin.

Wagman, D., Evans, W., Parker, V., Schumm, R., Halow, I., Bailey, S., Churney, K., Nuttall, R., 1982. The NBS tables of chemical thermodynamic properties. J. Phys. Chem. Ref. Data 11 (2), 302.

Zhu, H., Gu, X., Yao, K., Gao, L., Chen, J., 2009. Large-scale synthesis of $MgCl_2.6NH_3$ as an ammonia storage material. Ind. Eng. Chem. Res. 48 (11), 5317–5320.

Zondag, H.A., Essen, V.M.V., Bakker, M., 2010. Application of $MgCl_2.6H_2O$ for thermochemical seasonal solar heat storage. In: 5th International Renewable Energy, November.